The dynamics of spectral transfer in a model of drift wave turbulence with two nonlinearities

D. E. Newman and P. W. Terry
Department of Physics, University of Wisconsin–Madison, Madison, Wisconsin 53706

P. H. Diamond[a] and Y.-M. Liang
Department of Physics, University of California at San Diego, La Jolla, California 92093

(Received 1 July 1992; accepted 3 December 1992)

The spectral transfer dynamics of two-dimensional (2-D) drift wave turbulence over a broad range incorporating long- and short-wavelength extremes is studied numerically in the context of dissipative trapped electron convective cell turbulence. The direction, locality, and isotropy of energy and enstrophy transfer in wave-number space are determined by examining energy and enstrophy transfer rates, the enstrophy generation rate, spectra, and the spectrum response to perturbative impulses. Energy transfer is characterized by two subranges, according to the dominant nonlinearity, and a dynamically complex crossover region dividing the subranges. In the long-wavelength $\mathbf{E}\times\mathbf{B}$ subrange, energy transfer is nonlocal and anisotropic, proceeding to shorter wavelengths with significant generation of enstrophy. In the short-wavelength polarization drift subrange, energy transfer is local and, in the absence of sources and sinks, is dominated by an inverse cascade, consistent with the near conservation of enstrophy on dynamical time scales. In the crossover region, there is isotropic nonlocal forward transfer, as well as cascading to long wavelength. A significant shift of the frequency spectrum peak in the crossover region is shown to result from the cross coupling of the two nonlinearities. The shift is in the electron diamagnetic direction and increases with increasing wave number, consistent with the behavior of the renormalized response function. The simulation model does not incorporate the effects of electron inertia, and therefore does not account for the feedback of the frequency shift on nonlinear mode stability. Nevertheless, the simulations provide numerical validation of many aspects of the accompanying analytical investigation [Liang *et al.*, Phys. Fluids B **5**, 1128 (1993)].

I. INTRODUCTION

Long-wavelength tokamak turbulence, particularly as it pertains to core fluctuations and confinement, is currently an area of active investigation, both by experiment and theory. Following nearly a decade of neglect, renewed interest in this subject has been stimulated by recent theoretical work on trapped ion turbulence[1,2] and the development of several new core fluctuation diagnostics.[3–6] Augmenting the long-standing results of far infrared (FIR) laser scattering, which show wave-number spectra with energy increasing toward the longest measured scales,[6] spatially well-resolved measurements from beam emission spectroscopy,[3] and correlation reflectometry[4] have recently produced preliminary indication of the existence of long-wavelength fluctuations in the core plasma and suggest interesting, albeit tentative, links to confinement.

Recent analytical work indicates that trapped ion convective cell turbulence is a viable candidate for long-wavelength fluctuation activity in hot, auxiliary heated core plasmas.[1] Beyond its promise as a core fluctuation and transport model, however, trapped ion convective cell turbulence provides an instructive paradigm for long-wavelength turbulence and the spectral transfer properties that ultimately govern its saturation, spectral distribution of energy, and transport.[1,2] Its usefulness as a paradigm follows in part from the fact that trapped ion convective cell turbulence can be described by a one-field fluid model, e.g., the Kadomtsev–Pogutse equation, thus allowing a succinct and transparent representation of the nonlinear mode-coupling process. More importantly, a generalization of the Kadomtsev–Pogutse model provides a mode-coupling representation with two nonlinearities, the $\mathbf{E}\times\mathbf{B}$ and polarization drift nonlinearities, and is therefore generic to drift-wave-type fluctuations. For example, the $\mathbf{E}\times\mathbf{B}$ and polarization drift nonlinearities are the nonlinearities that appear in the one-fluid description (Terry–Horton) of turbulence associated with dissipative trapped electron and universal modes.[7]

Previous theoretical and computational analysis of purely trapped ion convective cell turbulence has focused on the long-wavelength regime, where nonlinear transfer is dominated by the $\mathbf{E}\times\mathbf{B}$ nonlinearity. These studies have demonstrated that the transfer of energy in wave-number space is directed toward short wavelength. The direct cascade of energy is possible because the conservative transfer of energy is not subject to any additional constraints, i.e., besides the energy, the $\mathbf{E}\times\mathbf{B}$ nonlinearity conserves no other nontrivial quadratic quantity. In addition to a direct cascade of energy, the $\mathbf{E}\times\mathbf{B}$ nonlinearity produces energy transfer which is anisotropic[2] and highly nonlocal in wave-

[a]Also at General Atomics, La Jolla, California 92138.

 0899-8221/93/041140-14$06.00

number space.[1,2] The occurrence of strong nonlocal transfer is a marked departure from the self-similar cascade dynamics inherent in the scaling arguments of Kolmogorov. The anisotropy of transfer follows from an absence of symmetry induced by the $\mathbf{k}_y$ dependence of the nonadiabatic electron response in the $\mathbf{E}\times\mathbf{B}$ nonlinearity. The anisotropy manifests itself as a transfer which is strongly nonlocal in the $\mathbf{k}_y$ direction (cross-field direction perpendicular to the density gradient) but characterized by comparable local and nonlocal transfer rates in the $\mathbf{k}_x$ (gradient) direction.

The long-wavelength regime of trapped ion convective cell turbulence contrasts strongly with a more familiar drift wave turbulence paradigm, the Hasegawa–Mima model.[8] In the Hasegawa–Mima equation, neglect of nonadiabatic electron dynamics eliminates the $\mathbf{E}\times\mathbf{B}$ nonlinearity and leaves the polarization drift nonlinearity (normally subdominant to the $\mathbf{E}\times\mathbf{B}$ nonlinearity in the long-wavelength limit) as the sole spectral transfer mechanism. While the neglect of nonadiabatic electron dynamics excludes the possibility of describing either instability or transport, it does produce a model that is nearly isomorphic to the quasigeostrophic equation. Accordingly, *two* dynamical invariants are admitted by the polarization drift nonlinearity, i.e., the energy and the enstrophy, or mean squared vorticity. In order to satisfy both constraints, a dual cascade process is required with the energy undergoing an inverse cascade or transfer to long wavelength, as in two-dimensional Navier–Stokes turbulence. The cascade dynamics of the Hasegawa–Mima equation are representative of the conventional view of spectral energy transfer in 2-D plasma turbulence. In particular, the notions of the inverse cascade and local transfer in wave-number space are pervasive in heuristic descriptions of saturation and spectral dynamics.

With nonadiabatic electrons, spectral transfer is affected by both the $\mathbf{E}\times\mathbf{B}$ and polarization drift nonlinearities, and enstrophy conservation, in a strict sense, is broken. However, the polarization drift nonlinearity involves a higher derivative of the fluctuating potential than the $\mathbf{E}\times\mathbf{B}$ nonlinearity. Consequently, the magnitude of the polarization drift nonlinearity becomes much larger than the magnitude of the $\mathbf{E}\times\mathbf{B}$ nonlinearity at short wavelengths, while the opposite holds at long wavelengths. It would seem reasonable, therefore, to predict the existence of spectral ranges in the short- and long-wavelength limits of the spectrum in which the transfer dynamics is dominated by one or the other of the nonlinearities. This would mean there is a spectral range at long wavelengths where energy is transferred to smaller scales and in which the total enstrophy within the range evolves on the time scale of the nonlinear interaction. There would also be a range at short wavelengths where energy is transferred to larger scales and enstrophy is approximately conserved on the time scale of nonlinear interactions. One of the primary aims of this paper is the testing of this hypothesis and the characterization of spectral transfer properties in both the intermediate range where the two nonlinearities play an active role and over the larger spectrum as a whole. Such a study is of direct relevance to trapped ion and electron turbulence because the direct transfer of energy generated at long wavelengths ($\omega < \omega_{bi}$) will inevitably carry energy to a spectrum region where the polarization drift nonlinearity is important, i.e., the dissipative trapped electron mode (DTEM) regime where $\omega_{be} > \omega > \omega_{bi}$.

It is also of considerable interest to examine the interplay of the two disparate transfer processes in terms of the locality and anisotropy of spectral transfer. In particular, as mentioned above, the $\mathbf{E}\times\mathbf{B}$ nonlinearity, acting alone, is known to produce transfer that is both nonlocal and anisotropic.[1,2] On the other hand, the polarization drift nonlinearity is isotropic in form, and by analogy with the two-dimensional Navier–Stokes equation, should transfer energy locally in wave-number space,[9] consistent with the notion of a Kolmogorov-type similarity range and cascade.

In the present work, broadband nonlinear transfer dynamics is examined for dissipative trapped electron mode turbulence (DTEM), including both the $\mathbf{E}\times\mathbf{B}$ and polarization drift nonlinearities. This work is an outgrowth of a previous study which considered only the $\mathbf{E}\times\mathbf{B}$ nonlinearity,[2] and is based on numerical solution of a model equation utilizing direct measurement of local and nonlocal spectral transfer rates. The computational work is accomplished with a spectral code containing up to 41×41 modes. The simulations examine two general situations: (i) the relaxation of the spectral energy distribution from an initial finite-amplitude configuration in the absence of driving and damping, or (ii) the evolution and saturation of the spectrum starting from infinitesimal amplitudes under driving by unstable modes at low wave number and damped modes at high wave number. The first situation permits measurement of the nonlinear transfer rate independent of any particular wave-number space configuration of sources and sinks, consistent with a chosen general spectrum shape. This situation also enables comparison of the stationary spectrum achieved by relaxation from an initial state with the predictions of equilibrium statistical mechanics. The second situation addresses the transfer characteristic of the most likely arrangement of sources and sinks. In this case, the net energy transfer in a saturated state (assuming one occurs) is not in question, since it will necessarily proceed from source to sink. Rather, these studies will determine the spectrum shape and examine nonlinear transfer in subranges of wave-number space, focusing on the issues of direction, locality, and isotropy.

A striking visualization of the energy transfer in the saturated state may be produced by subjecting the saturated spectrum to a large, localized (in wave-number space) perturbation and observing the subsequent relaxation of the spectrum to its original stationary configuration. Using this technique it is possible to determine the direction, locality, and isotropy of transfer in various subranges of the spectrum. This technique is the spectral analog of perturbative transport studies using modulated gas feed, heat pulse propagation, etc., to infer the locality, direction, and magnitude of spatial transport. As such, it represents a reasonably accessible means of examining spectral transfer and cascades in experiment. Tests of this

technique in simulated turbulence are reported herein.

The principal results of this paper are now summarized. It is found that the polarization drift nonlinearity, acting alone, produces transfer that is both isotropic and local. Both properties follow directly from symmetries of the nonlinearity that are not present in the pure Kadomtsev–Pogutse model. With both nonlinearities acting simultaneously, subranges exist in which the transfer is virtually indistinguishable from the transfer of the dominant nonlinearity, if acting alone. Enstrophy generation is shown to be an effective indicator of the dominance of one nonlinearity over the other in these cases. If the maximum and minimum wave numbers restrict the spectrum to a range where the $\mathbf{E}\times\mathbf{B}$ nonlinearity dominates throughout, enstrophy production is significant and increases on a time scale of a few eddy turnover times. Energy is transferred to high $\mathbf{k}$ in an anisotropic and nonlocal process characteristic of cases in which the polarization drift nonlinearity is entirely absent. If the spectrum is fixed to a range in which the polarization drift nonlinearity dominates throughout, enstrophy production is weak, with an e-folding time much larger than the eddy turnover time. Here, a dual cascade is evident and transfer is isotropic and local. A third subrange exists and is accessed by determining the maximum and minimum wave numbers so that both nonlinearities are roughly comparable over most of the spectrum (i.e., neither dominates). In this subrange, enstrophy production is moderate. Spectral transfer tends to be isotropic but retains a strong nonlocal component. In this situation, the local transfer develops an anisotropy which offsets the anisotropy of the nonlocal flow. When undriven, undamped turbulence evolves from an initial spectrum peaked at low $\mathbf{k}$, the spectrum relaxes to a time-asymptotic state that remains peaked at long wavelength but has two subranges with distinct spectral falloff rates. The subranges separate at the point where the two nonlinearities are equal, with a slightly steeper slope in the high-$\mathbf{k}$ range than in the low-$\mathbf{k}$ range. Energy flow is toward higher $\mathbf{k}$ in the low-$\mathbf{k}$ subrange, with the converse true in the high-$\mathbf{k}$ subrange. Present limits on $\mathbf{k}$ space resolution make it difficult to extend this subrange to sufficiently large and small wave number to allow each nonlinearity to dominate at the extremes of the spectrum. It is anticipated that a larger subrange would accentuate, in each of its extremes, both the spectrum falloff disparity and the differences in energy transfer direction.

For turbulence driven by unstable modes at long wavelength and damped by a hyperviscous damping at small wavelength, there is a noticeable difference between the wave-number spectra that occur when either of the nonlinearities is acting alone and the spectrum that occurs in the subrange when both nonlinearities are present and comparable. Whereas the spectrum of the $\mathbf{E}\times\mathbf{B}$ nonlinearity tends to be flat,[2] it falls off toward high k with both nonlinearities. There is a discernible change in the falloff rate at the wave number where the two nonlinearities are equal, with a flatter falloff in the longer-wavelength part of the spectrum. Distinct differences in the transfer rate are observed. In interpreting the transfer diagnostics, it appears that transfer is more sensitive to the cross coupling of the nonlinearities than is the spectrum. Consequently, transfer behavior in either subrange with the unmodified signature of the dominant nonlinearity is more difficult to discern in the relatively small wave-number space of the present simulations. Nevertheless, the following statements represent the qualitative behavior of the transfer with both nonlinearities in the steady state. In the $\mathbf{E}\times\mathbf{B}$ subrange, transfer is nonlocal. Above a critical wave number (related to the wave number where the two nonlinearities are equal), nonlocal transfer becomes weak relative to the total transfer. Thus there is a polarization subrange with local transfer. A dual cascade is evident in this region of $\mathbf{k}$ space and accounts for the change in spectral index in crossing from one subrange to the other.

A novel and potentially important aspect of the interplay between the two nonlinearities is evident in the frequency spectra of individual modes. In the regime where both nonlinearities are comparable, a large shift of the frequency spectrum peak is observed. For shorter-wavelength modes, the shift is to higher frequency and can be many times the diamagnetic frequency. If either nonlinearity is absent, or contributes only weakly to the transfer dynamics, the shift is small. Theoretically, a spectrum shift is found in the renormalized response function.[10] This shift arises from the cross coupling of the nonlinearities through the driven fluctuations. Since the $\mathbf{E}\times\mathbf{B}$ nonlinearity has one fewer spatial derivative than the polarization drift nonlinearity, the cross-coupling term is 90° out of phase with the eddy damping decrement, and thus enters as a shift in the spectrum peak (as opposed to a broadening). The occurrence of a frequency shift has a potentially significant impact on stability and transport,[10] as well as the interpretation of fluctuation measurements. A derivation of the frequency shift and its effect on nonlinear stability, and therefore on the spectrum, is explored in the article immediately preceding this one (Ref. 10). While this and the preceding article are intended as analytical and computational counterparts, the present work is restricted to observational analysis of the spectrum shift. The self-consistent effect of the shift on mode fluctuation levels cannot be described by the present computational model, and will be addressed in future work.

The paper is organized as follows. The model and its properties are presented and discussed in Sec. II. In Sec. III, we describe the spectral transfer properties. To facilitate interpretation of the results, a subsection examines the locality and isotropy of transfer of the polarization drift nonlinearity. In Sec. IV, measurements of the frequency spectrum are presented and discussed. The conclusions are given in Sec. V.

II. BASIC MODEL AND PROPERTIES

In this section the basic model is presented and the dynamical coupling of the two nonlinearities is analyzed from the perspective of the mathematical structure of the model. This analysis examines integral invariants, symmetries in the structure of the nonlinearities, and the renormalized mode equations.

The model utilized for this study is a trapped particle fluid equation. This model couples the laminar dynamics of collisional trapped electrons with hydrodynamic ions through the quasineutrality condition. The derivation of this equation and a discussion of its details and limitations have been presented elsewhere.[1,2,7,10] In previous work, the polarization drift nonlinearity was neglected by considering only the long-wavelength extreme of the spectrum.[1,2] Here, the polarization drift nonlinearity is included, yielding the model equation

$$\frac{\partial \tilde{n}}{\partial t}+D\frac{\partial^2 \tilde{n}}{\partial y^2}+V_D\frac{\partial \tilde{n}}{\partial y}+\nu_i\tilde{n}-L_nD\nabla\frac{\partial \tilde{n}}{\partial y}\times\mathbf{z}\cdot\nabla\tilde{n}$$

$$+\rho_sC_s\nabla\tilde{n}\times\mathbf{z}\cdot\nabla\rho_s^2\nabla^2\tilde{n}+\mu\nabla^4\tilde{n}=0, \tag{1}$$

where $\tilde{n}$ is the fluctuating ion density, $V_D=(cT_e/eB)L_n^{-1}$ is the diamagnetic drift velocity, $D=\varepsilon^{1/2}V_D{}^2(1+3\eta_e/2)/\nu_{\mathrm{eff},e}$ is a negative diffusivity describing the destabilization of DTEM modes by electron collisions, ε is the trapped electron fraction, $\eta_e=d\ln T/d\ln n$ is the electron temperature gradient parameter, ν_i models long-wavelength collisional damping, $\nu_{\mathrm{eff},e}=\nu_e/\varepsilon$, μ is the coefficient of the hyperviscosity introduced to model strong damping at high k, L_n is the density gradient scale length, $\rho_s=(cT_e/eB)/C_s$ is the ion gyroradius evaluated at the electron temperature, and $C_s=(T_e/m_i)^{1/2}$ is the ion sound speed. In keeping with the emphasis of the present paper on nonlinear transfer effects, the linear polarization drift term responsible for linear dispersion has not been included in Eq. (1). This allows significant savings in computation time. Inclusion of this term introduces straightforward modifications of subsequent equations and relations (for example, the energy and enstrophy defined below are modified when dispersion is included[10]). However, the basic mechanisms governing transfer and the concepts describing this process are unaltered. Indeed, numerical solutions with and without the linear polarization term included were found to be qualitatively the same for spectral ranges studied herein.

The first nonlinearity appearing in Eq. (1) is the **E×B** nonlinearity, arising from $\mathbf{v}_E\cdot\nabla\tilde{n}_i$, where $\mathbf{v}_E=-(c/B_0)\nabla\phi\times\mathbf{z}$ is the **E×B** drift. The second nonlinearity is the polarization drift nonlinearity, and arises from $n_0\nabla\cdot\mathbf{v}_p^{(1)}$, where $\mathbf{v}_p^{(1)}=B_0{}^{-1}(m_ic/e)\mathbf{z}\times\mathbf{v}_E\cdot\nabla\mathbf{v}_E$ is the nonlinear polarization drift. The **E×B** nonlinearity requires a nonadiabatic electron response (provided by the trapped electrons), whereas the polarization drift nonlinearity derives from the ion polarization drift.

From Eq. (1), it is apparent that, by virtue of its additional spatial derivative, the polarization drift nonlinearity dominates the **E×B** nonlinearity at very short wavelengths. The converse holds at long wavelengths. The nominal crossover point is given by the wave number at which the two nonlinearities are equal. Assuming rough isotropy, so that $\nabla_\perp\approx\partial/\partial y$, this wave number is given by $\mathbf{k}\rho_s\approx\delta=C_s/L_n\nu_{\mathrm{eff},e}\equiv\mathbf{k}_0\rho_s$. Because the nonlinearities are characterized, not by a single spatial scale, but, by a triad interaction consisting of three waves of differing wavelengths, it is more realistic to identify a region, centered about the crossover wave number, in which the two nonlinearities are comparable, rather than to speak of a single wave number at which the two are equal.

Because of the presence of the **E×B** nonlinearity, a single quadratic invariant, the energy, is admitted by Eq. (1) in the absence of driving and damping, i.e.,

$$\frac{1}{2}\frac{\partial}{\partial t}\int\tilde{n}^2\,d^2x=D\int\left(\frac{\partial\tilde{n}}{\partial y}\right)^2d^2x-\nu_{\mathrm{eff},i}\int\tilde{n}^2\,d^2x$$

$$-\mu\int(\nabla^2\tilde{n})^2\,d^2x, \tag{2}$$

where $E=\int\tilde{n}^2\,d^2x$ is the energy and the terms on the right-hand side represent the dissipative source (inverse electron damping) and sinks (ion–ion collisions and hyperviscosity). Only if the **E×B** nonlinearity is absent, is there a second invariant, the enstrophy, defined by $\Omega=\int|\nabla\tilde{n}|^2\,d^2x$. From Eq. (1), the enstrophy evolution is given by

$$\frac{1}{2}\frac{\partial}{\partial t}\int|\nabla\tilde{n}|^2\,d^2x-D\int\left|\nabla\frac{\partial\tilde{n}}{\partial y}\right|^2d^2x+\nu_{\mathrm{eff},i}\int|\nabla\tilde{n}|^2\,d^2x$$

$$+\mu\int(\nabla^3\tilde{n})^2\,d^2x=-L_nD\int\nabla^2\tilde{n}\nabla\frac{\partial\tilde{n}}{\partial y}\times\mathbf{z}\cdot\nabla\tilde{n}\,d^2x. \tag{3}$$

The term on the right-hand side describes the generation or destruction of enstrophy associated with the conservative transfer of energy by the **E×B** nonlinearity. As previously indicated, the **E×B** nonlinearity in isolation transfers energy to short wavelengths, given a spectrum that is peaked at long wavelength or flat, and therefore drives robust production of enstrophy.[2] This term is present even in spectral ranges where the polarization drift nonlinearity dominates ($\mathbf{k}>\mathbf{k}_0$). Consequently, enstrophy is not conserved even when the **E×B** nonlinearity is weak compared to the polarization drift nonlinearity. However, in such a case, the **E×B** nonlinearity accounts for proportionately less of the total energy transfer. Because enstrophy production is tied to energy transfer by the **E×B** nonlinearity, it can be expected that the importance of enstrophy production in the cascade dynamics diminishes for $k>k_0$. This fact is also apparent in comparing the enstrophy production rate

$$\gamma_\Omega=\left(\frac{1}{2}\int|\nabla\tilde{n}|^2\,d^2x\right)^{-1}L_nD\int\nabla^2\tilde{n}\nabla\frac{\partial\tilde{n}}{\partial y}\times\mathbf{z}\cdot\nabla\tilde{n}\,d^2x, \tag{4}$$

with the nonlinear interaction rate or eddy turnover rate. For $\mathbf{k}<\mathbf{k}_0$, the eddy turnover rate is controlled by the dominant **E×B** nonlinearity and can be expected to be comparable to the enstrophy generation rate. For $k>k_0$ the eddy turnover rate is controlled by the larger polarization drift nonlinearity, while the enstrophy generation rate is tied to the weaker **E×B** nonlinearity. Consequently, there will be little enstrophy generation on the nonlinear interaction or nonlinear transfer time scale. This fact suggests a convenient diagnostic of the strength of the polarization drift nonlinearity in the form of the enstrophy dissipation rate $\hat{\gamma}_\Omega$ normalized to the mean oscillation time of

an intermediate scale mode. Results from the simulations will show $\hat{\gamma}_\Omega{}^{-1}$ to range from 2–3 in the $\mathbf{E}\times\mathbf{B}$ subrange to hundreds in the polarization subrange.

Energy transfer that is anisotropic and nonlocal in wave-number space is a robust feature of the $\mathbf{E}\times\mathbf{B}$ nonlinearity, but at variance with the conventional picture of the cascade process. On the other hand, the polarization drift nonlinearity is of the same form as the advective nonlinearity of the vorticity evolution equation of Navier–Stokes turbulence. Therefore it is reasonable to postulate that the polarization drift nonlinearity produces transfer which is local and isotropic. It is possible to associate these features with symmetries in the structure of the nonlinear coupling. These symmetries are most transparent in the Fourier representation of the nonlinearities. Transforming Eq. (1), the evolution of mode amplitudes is given by

$$\frac{\partial\tilde{n}_\mathbf{k}}{\partial t}-D\mathbf{k}_y{}^2\tilde{n}_\mathbf{k}+iV_D\mathbf{k}_y\tilde{n}_\mathbf{k}+\nu_{\mathrm{eff},i}\tilde{n}_\mathbf{k}+\mu\mathbf{k}^4\tilde{n}_\mathbf{k}$$
$$+N_\mathbf{k}{}^{(\mathbf{E}\times\mathbf{B})}+N_\mathbf{k}{}^{(\mathrm{Pol})}=0, \tag{5}$$

where

$$N_\mathbf{k}{}^{(\mathbf{E}\times\mathbf{B})}=\frac{i}{2}L_nD\sum_{\mathbf{k}'}\mathbf{k}\times\mathbf{k}'\mathbf{z}[\mathbf{k}_y'-(\mathbf{k}_y-\mathbf{k}_y')]\tilde{n}_{\mathbf{k}'}\tilde{n}_{\mathbf{k}-\mathbf{k}'}$$
$$\equiv\sum_{\mathbf{k}'}\chi^{(\mathbf{E}\times\mathbf{B})}_{\mathbf{k},\mathbf{k}'}\tilde{n}_{\mathbf{k}'}\tilde{n}_{\mathbf{k}-\mathbf{k}'}, \tag{6}$$

$$N_\mathbf{k}{}^{(\mathrm{Pol})}=\frac{1}{2}\rho_s{}^3C_s\sum_{\mathbf{k}'}\mathbf{k}\times\mathbf{k}'\cdot\mathbf{z}[(\mathbf{k}_\perp-\mathbf{k}_\perp')^2-\mathbf{k}_\perp'^2]\tilde{n}_{\mathbf{k}'}\tilde{n}_{\mathbf{k}-\mathbf{k}'}$$
$$\equiv\sum_{\mathbf{k}'}\chi^{(\mathrm{Pol})}_{\mathbf{k},\mathbf{k}'}\tilde{n}_{\mathbf{k}'}\tilde{n}_{\mathbf{k}-\mathbf{k}'}. \tag{7}$$

From Eqs. (6) and (7), the lack of anisotropy in the $\mathbf{E}\times\mathbf{B}$ nonlinearity is evident in the appearance of the factor $\mathbf{k}_y'-(\mathbf{k}_y-\mathbf{k}_y')$, whereas the polarization drift nonlinearity is manifestly isotropic. (In comparing expressions in this paper with those of the accompanying paper by Liang *et al.*,[10] it should be noted that $\mathbf{k}-\mathbf{k}'$ here is identical with $\mathbf{k}''$ in the accompanying paper.)

Differences between the two nonlinearities regarding the locality of transfer in wave-number space can also be deduced from Eqs. (6) and (7). From Eq. (6), the $\mathbf{E}\times\mathbf{B}$ coupling is proportional to $\mathbf{k}_y'-(\mathbf{k}_y-\mathbf{k}_y')=2\mathbf{k}_y'-\mathbf{k}_y$. For a nonlocal triad consisting of a long-wavelength fluctuation $\mathbf{k}_y$ interacting with short wavelength fluctuations $\mathbf{k}_y'$ and $\mathbf{k}_y-\mathbf{k}_y'$ ($\mathbf{k}_y\ll\mathbf{k}_y'$, $\mathbf{k}_y-\mathbf{k}_y'$), this factor is proportional to the large wave number $2\mathbf{k}_y'$. For local triads ($\mathbf{k}_y\sim\mathbf{k}_y'\sim\mathbf{k}_y-\mathbf{k}_y'$), $2\mathbf{k}_y'-\mathbf{k}_y\sim\mathbf{k}_y$, i.e., the factor is proportional to the small wave number. Clearly, the $\mathbf{E}\times\mathbf{B}$ coupling favors nonlocal interaction. Note that this predilection for nonlocal coupling is not isotropic, but applies solely to the displacement in the $\mathbf{k}_y$ direction. By contrast, the comparable coupling factor in the polarization drift nonlinearity is $(\mathbf{k}_\perp-\mathbf{k}_\perp')^2-\mathbf{k}_\perp'^2\sim\mathbf{k}_\perp{}^2$ (spectrum symmetries eliminate the contribution $-2\mathbf{k}_\perp\mathbf{k}_\perp'$). Because this factor involves the squares of the wave numbers $\mathbf{k}_\perp'$ and $\mathbf{k}_\perp-\mathbf{k}_\perp'$, the large wave number $\mathbf{k}_\perp'^2$ cancels and the factor is proportional to the small wave number $\mathbf{k}_\perp{}^2$. Hence the polarization drift nonlinearity, unlike the $\mathbf{E}\times\mathbf{B}$ nonlinearity, has no special weighting that favors nonlocal coupling (beyond the universal factors $\mathbf{k}\times\mathbf{k}'\cdot\mathbf{z}$ and the spectral energy distribution $\tilde{n}_{\mathbf{k}'}\tilde{n}_{\mathbf{k}-\mathbf{k}'}$). The symmetries in the nonlinear couplings responsible for this distinction between the $\mathbf{E}\times\mathbf{B}$ and polarization drift nonlinearities derive from the nonadiabatic electron response of the $\mathbf{E}\times\mathbf{B}$ nonlinearity ($\phi\sim\delta\partial\tilde{n}_e/\partial y$) and the adiabatic electron response of the polarization drift nonlinearity ($\phi\sim\tilde{n}$). These symmetries carry directly over to the energy transfer rates and give rise to a nonlocal transfer rate by the $\mathbf{E}\times\mathbf{B}$ nonlinearity which dramatically exceeds the local transfer rate, while for the polarization drift nonlinearity, local and nonlocal transfer rates tend to be comparable.

The existence of the frequency spectrum shift is also apparent from Eqs. (6) and (7) under iteration of the $\tilde{n}_{\mathbf{k}-\mathbf{k}'}$ factor in each expression. In the iteration procedure, $\tilde{n}_{\mathbf{k}-\mathbf{k}'}$ is replaced by the formal solution of Eq. (5) (with $\mathbf{k}\to\mathbf{k}-\mathbf{k}'$). This solution is obtained by placing $N^{(\mathbf{E}\times\mathbf{B})}_{\mathbf{k}-\mathbf{k}'}+N^{(\mathrm{Pol})}_{\mathbf{k}-\mathbf{k}'}$ on the right-hand side of Eq. (5) and inverting the temporal operator of the left-hand side. Under standard statistical closures, the sum in the $N_{\mathbf{k}-\mathbf{k}'}$ terms of Eq. (5) is restricted to the directly interacting triplet giving

$$\tilde{n}_{\mathbf{k}-\mathbf{k}'}=-2\Delta\omega_{\mathbf{k}-\mathbf{k}'}{}^{-1}(\chi^{(\mathrm{Pol})}_{\mathbf{k}-\mathbf{k}',-\mathbf{k}'}+\chi^{(\mathbf{E}\times\mathbf{B})}_{\mathbf{k}-\mathbf{k}',-\mathbf{k}'})\tilde{n}_{-\mathbf{k}'}\tilde{n}_\mathbf{k}, \tag{8}$$

where $\Delta\omega_\mathbf{k}{}^{-1}$ is the inversion of the first four terms of Eq. (4). Substitution of Eq. (10) into Eqs. (6) and (7) gives the coherent nonlinear response from each of the nonlinearities. Combining, $\tilde{n}_\mathbf{k}$ evolves according to

$$\frac{\partial\tilde{n}_\mathbf{k}}{\partial t}-D\mathbf{k}_y{}^2\tilde{n}_\mathbf{k}+\frac{iV_D}{2}\mathbf{k}_y\tilde{n}_\mathbf{k}+\nu_{\mathrm{eff},i}\tilde{n}_\mathbf{k}+\mu\mathbf{k}^4\tilde{n}_\mathbf{k}-\nu_\mathbf{k}{}^{nl}\tilde{n}_\mathbf{k}=0, \tag{9}$$

where

$$\nu_\mathbf{k}{}^{nl}=2\sum_{\mathbf{k}'}(\chi^{(\mathrm{Pol})}_{\mathbf{k},\mathbf{k}'}+\chi^{(\mathbf{E}\times\mathbf{B})}_{\mathbf{k},\mathbf{k}'})(\chi^{(\mathrm{Pol})}_{\mathbf{k}-\mathbf{k}',-\mathbf{k}'}$$
$$+\chi^{(\mathbf{E}\times\mathbf{B})}_{\mathbf{k}-\mathbf{k}',-\mathbf{k}'})|\tilde{n}_{-\mathbf{k}'}|^2. \tag{10}$$

Note that $\chi^{(\mathrm{Pol})}$ is 90° out of phase with $\chi^{(\mathbf{E}\times\mathbf{B})}$. Consequently, the diagonal terms $\chi^{(\mathbf{E}\times\mathbf{B})}_{\mathbf{k},\mathbf{k}'}\chi^{(\mathbf{E}\times\mathbf{B})}_{\mathbf{k}-\mathbf{k}',-\mathbf{k}'}$ and $\chi^{(\mathrm{Pol})}_{\mathbf{k},\mathbf{k}'}\chi^{(\mathrm{Pol})}_{\mathbf{k}-\mathbf{k}',-\mathbf{k}'}$ produce coherent damping while the off-diagonal terms $\chi^{(\mathbf{E}\times\mathbf{B})}_{\mathbf{k},\mathbf{k}'}\chi^{(\mathrm{Pol})}_{\mathbf{k}-\mathbf{k}',-\mathbf{k}'}$ and $\chi^{(\mathrm{Pol})}_{\mathbf{k},\mathbf{k}'}\chi^{(\mathbf{E}\times\mathbf{B})}_{\mathbf{k}-\mathbf{k}',-\mathbf{k}'}$ produce a phase oscillation. Accordingly, the diagonal terms are related to the spectrum linewidth[11] while the off-diagonal terms contribute to the frequency of the spectrum peak.[10] Physically, the frequency shift arises from the interaction of a driven fluctuation $\tilde{n}_{\mathbf{k}-\mathbf{k}'}$ which is 90° out of phase with the test and beat waves at $\mathbf{k}$ and $\mathbf{k}'$. Clearly, it is cross-coupling of modes driven by each of the two nonlinearities that produces the shift, with no shift occurring if either of the nonlinearities is absent.

Substituting for $\chi^{(\mathbf{E}\times\mathbf{B})}$ and $\chi^{(\mathrm{Pol})}$ in Eq. (10), it is seen that

$$\mathrm{Im}\,\nu_{\mathbf{k}}^{nl} = -L_n D \rho_s^3 C_s \sum_{\mathbf{k}'} (\mathbf{k}\times\mathbf{k}'\cdot\mathbf{z})^2 \mathbf{k}_y \times [2\mathbf{k}_\perp^{\,2} - \mathbf{k}_\perp'^{\,2}]\,|n_{\mathbf{k}'}|^2, \tag{11}$$

corresponding to an upshift for intermediate modes $\mathbf{k}_\perp^{\,2} \gtrsim \langle \mathbf{k}_\perp^{\,2} \rangle$. The qualitative features of this predicted shift, specifically its sign and its $\mathbf{k}_y$ dependence, will be examined in Sec. IV.

III. SPECTRAL TRANSFER

In this section the spectral flow of energy over the spectrum range is described. The transfer properties are inferred from the time evolution of the wave-number spectrum and the time evolution of the energy and enstrophy transfer rates from (or to) selected bands in wave-number space.[2] The energy and enstrophy transfer rates due to the $\mathbf{E}\times\mathbf{B}$ nonlinearity are given in Ref. 2. With the addition of the polarization drift nonlinearity, the evolution of the energy and enstrophy of the mode $\mathbf{k}$ is described by

$$\frac{1}{2}\frac{\partial|\tilde{n}_{\mathbf{k}}|^2}{\partial t} - D\mathbf{k}_y^2|\tilde{n}_{\mathbf{k}}|^2 + \nu_{\mathrm{eff},i}|\tilde{n}_{\mathbf{k}}|^2 + \mu\mathbf{k}^4|\tilde{n}_{\mathbf{k}}|^2 = T_{\mathbf{k}}, \tag{12}$$

$$\frac{1}{2}\frac{\partial\mathbf{k}^2|\tilde{n}_{\mathbf{k}}|^2}{\partial t} - D\mathbf{k}_y^2\mathbf{k}^2|\tilde{n}_{\mathbf{k}}|^2 + \nu_{\mathrm{eff},i}\mathbf{k}^2|\tilde{n}_{\mathbf{k}}|^2 + \mu\mathbf{k}^6|\tilde{n}_{\mathbf{k}}|^2 = U_{\mathbf{k}}, \tag{13}$$

where

$$T_{\mathbf{k}} = L_n D\,\mathrm{Im}\sum_{\mathbf{k}'} (\mathbf{k}\times\mathbf{k}'\cdot\mathbf{z})\mathbf{k}_y'\tilde{n}_{\mathbf{k}'}\tilde{n}_{\mathbf{k}-\mathbf{k}'}\tilde{n}_{\mathbf{k}}^* - \rho_s^3 C_s\,\mathrm{Re}\sum_{\mathbf{k}'} \mathbf{k}\times\mathbf{k}'\cdot\mathbf{z}(\mathbf{k}_\perp - \mathbf{k}_\perp')^2\tilde{n}_{\mathbf{k}'}\tilde{n}_{\mathbf{k}-\mathbf{k}'}\tilde{n}_{\mathbf{k}}^* \tag{14}$$

and

$$U_{\mathbf{k}} = L_n D\,\mathrm{Im}\sum_{\mathbf{k}'} (\mathbf{k}\times\mathbf{k}'\cdot\mathbf{z})\mathbf{k}^2\mathbf{k}_y'\tilde{n}_{\mathbf{k}'}\tilde{n}_{\mathbf{k}-\mathbf{k}'}\tilde{n}_{\mathbf{k}}^* - \rho_s^3 C_s \times \mathrm{Re}\sum_{\mathbf{k}'} \mathbf{k}\times\mathbf{k}'\cdot\mathbf{z}\mathbf{k}^2(\mathbf{k}_\perp - \mathbf{k}_\perp')^2\tilde{n}_{\mathbf{k}'}\tilde{n}_{\mathbf{k}-\mathbf{k}'}\tilde{n}_{\mathbf{k}}^* \tag{15}$$

are, respectively, the energy and enstrophy transfer rates from the mode $\mathbf{k}$. Note that summing $U_{\mathbf{k}}$ over all $\mathbf{k}$ yields the enstrophy production rate, Eq. (4). Summing $T_{\mathbf{k}}$ and $U_{\mathbf{k}}$ over a band of wave numbers (typically with $\mathbf{k}_y$=const or $\mathbf{k}_x$=const) yields the transfer from the given band. Moreover, by selecting only certain $\mathbf{k}'$ values in the sums, the transfer rates can be formulated to identify transfer between coupled triplets with wave numbers that span more than a significant fraction of the spectrum (typically $\frac{1}{3}$ to $\frac{1}{2}$). This allows a quantitative assessment of the relative magnitudes of local and nonlocal transfer. Before describing the flow induced by the $\mathbf{E}\times\mathbf{B}$ and polarization drift nonlinearities together, it is useful to establish a reference in terms of the flow properties under each of the nonlinearities in isolation.

A. Transfer properties of each nonlinearity in isolation

Spectral flow by the $\mathbf{E}\times\mathbf{B}$ nonlinearity was described in Ref. 2 and is briefly summarized. In the absence of driving and damping, spectra initially peaked at low $\mathbf{k}$ relax to the equipartitioned state predicted by statistical mechanics. The relaxation is accomplished by a prompt nonlocal flow to the largest $\mathbf{k}_y$ bands (defined by $\mathbf{k}_y \sim \mathbf{k}_{y\max}$), producing, within a few eddy turnover times, spectra with peaks at high $|\mathbf{k}_y|$. Subsequent sloshing motion excites the intermediate wave numbers. The energy transfer rate between nonlocally displaced $\mathbf{k}_y$ bands exceeds the transfer between closely neighboring (local) bands by an order of magnitude. Local and nonlocal transfer rates in the $\mathbf{k}_x$ direction are comparable. In both directions, transfer proceeds to high $\mathbf{k}$ when the spectrum is initially peaked. When driven by modes at low $\mathbf{k}$ and damped by modes at high $\mathbf{k}$ with an intermediate inertial range, the stationary wave-number spectrum is remarkably flat over the inertial range, falling off only at the damped modes. This dramatic deviation of the spectrum from that predicted by similarity arguments is another indication of strong nonlocal transfer.

When the polarization drift nonlinearity is the sole nonlinear coupling mechanism, the equilibrium spectrum peaks at low $\mathbf{k}$. Figure 1 shows the equilibrium spectrum (no driving or damping) reached from an initial spectrum with $|n_{\mathbf{k}}|^2 \sim \mathbf{k}^{-3}$ for 41×41 modes. Relative to the initial spectrum, the equilibrium spectrum is more peaked at lower wave numbers and flatter at large wave numbers, indicating an inverse cascade of energy to low $\mathbf{k}$, but also some energy transfer to high $\mathbf{k}$. Indeed, the energy transfer rate reveals such a transfer pattern. From Fig. 2, the transfer rate $T_{\mathbf{k}}$ is positive at the lowest wave numbers and negative somewhat higher, indicating a primary transfer into the lowest wave numbers from the higher band. The higher band also engages in a smaller subsidiary transfer to even higher wave numbers, as seen in the positive peak just above the negative feature. In the upper half of the spectrum, there is little net transfer above the noise level as defined by the standard deviation of the scatter in the transfer history.

The transfer to low $\mathbf{k}$ is consistent with the dynamical constraints imposed by the conservation of energy and enstrophy. The smaller forward cascade might appear to be a violation of these constraints. However, as shown elsewhere,[12] some energy must be transferred in the forward direction in order to generate sufficient enstrophy to compensate for the enstrophy destroyed by the inverse energy cascade. The amount of energy transferred to high $\mathbf{k}$ decreases to zero as the largest wave number goes to infinity. For the rather small wave-number spaces considered here, however, this energy can be appreciable. This process contributes to the existence of two falloff rates in the equilibrium spectrum, a feature not anticipated by equilibrium statistical mechanics.

As discussed in the previous section, the symmetries of the coupling coefficient of the polarization drift nonlinearity suggest that nonlocal transfer should be no larger than

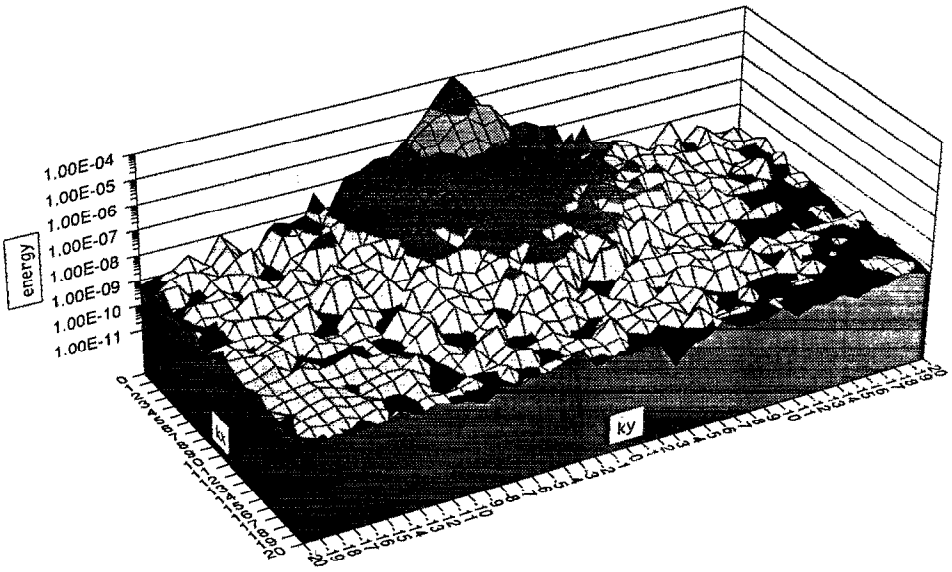

FIG. 1. Equilibrium spectrum of undriven/undamped turbulence with only the polarization drift nonlinearity. This spectrum is the relaxed state that has evolved from an initial spectrum with a fall-off index of $\alpha = -4$. The initial spectrum is identical to the initial spectrum shown in Fig. 1 of Ref. 2.

the local transfer. In fact, as evidenced by Fig. 3, the local transfer rate from the band with negative transfer in Fig. 2 exceeds the nonlocal transfer rate by a factor of 2 or 3. Moreover, the transfer rates in the $\mathbf{k}_x$ and $\mathbf{k}_y$ directions are found to be comparable to within a factor of 2, so that transfer is isotropic, as anticipated from the form of the nonlinearity.

B. Transfer properties with both nonlinearities

With both nonlinearities present, the transfer of energy and enstrophy is characterized by three general principles. These are now presented. (1) Excepting the effects represented by the other two principles, each nonlinearity transfers energy and enstrophy throughout the spectrum as it would if acting alone. Because the $\mathbf{E}\times\mathbf{B}$ nonlinearity dominates at low $\mathbf{k}(\mathbf{k}<\mathbf{k}_0)$, the net transfer in the long-wavelength subrange is similar to that produced by the $\mathbf{E}\times\mathbf{B}$ nonlinearity alone, i.e., the transfer is to high $\mathbf{k}$ with a strong nonlocal component in $\mathbf{k}_y$. While the $\mathbf{E}\times\mathbf{B}$ dynamics is similar in the high-k subrange, the transfer they produce is small by comparison with that of the polarization drift nonlinearity, which drives a dual cascade via local isotropic transfer.

(2) With the two nonlinearities acting together, the spectral distribution of energy $|\tilde{n}_{\mathbf{k}}|^2$ is modified relative to its configuration with a single nonlinearity. Since $T_{\mathbf{k}}$ and $U_{\mathbf{k}}$ depend on amplitudes $\tilde{n}_{\mathbf{k}'}$, $\tilde{n}_{\mathbf{k}-\mathbf{k}'}$, and $\tilde{n}_{\mathbf{k}}{}^*$ [Eqs. (14) and (15)], the transfer is also modified relative to its behavior for a single nonlinearity. In each of the subranges, the spectra, both the equilibrium and the driven/damped stationary spectrum, tend to look like the spectra of the dominant nonlinearity, when acting alone. Consequently,

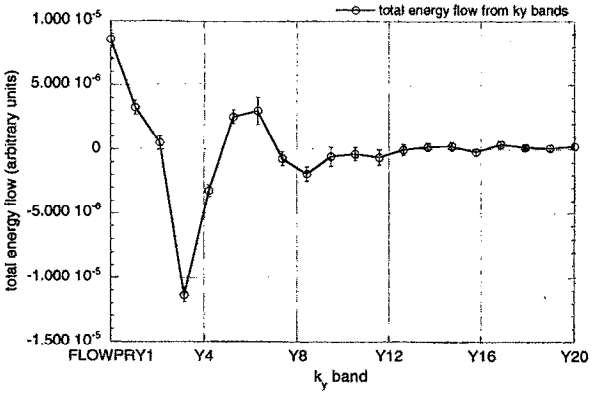

FIG. 2. Time-averaged energy transfer rate during the relaxation leading to the spectrum of Fig. 1. The error bars indicate the standard deviation from the mean value plotted in the figure.

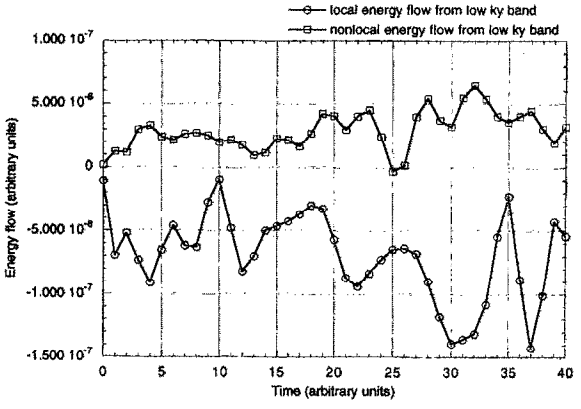

FIG. 3. Local and nonlocal energy transfer rates from the band with negative transfer (energy outflow) during the relaxation leading to the spectrum of Fig. 1.

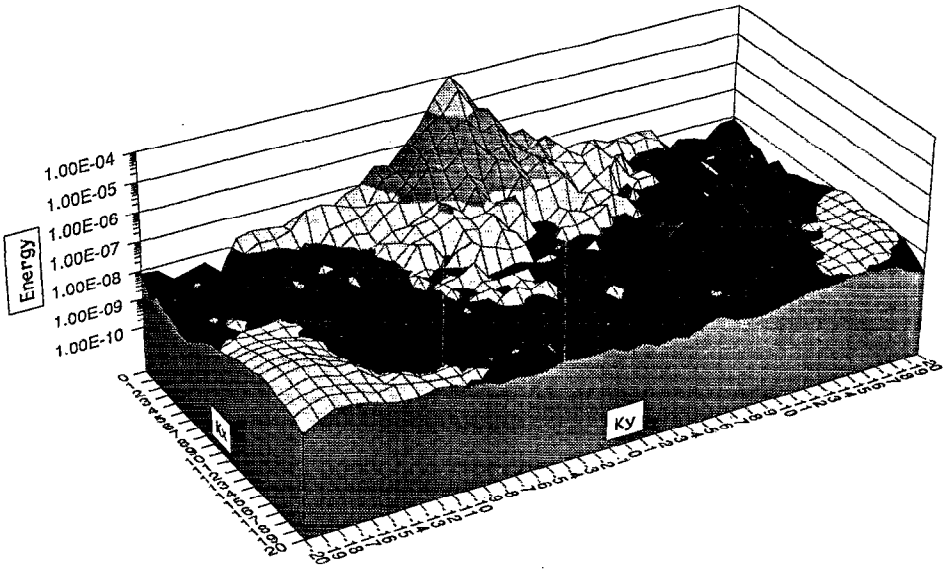

FIG. 4. Spectrum of undriven/undamped turbulence with both the $\mathbf{E}\times\mathbf{B}$ and polarization drift nonlinearities ($\mathbf{E}\times\mathbf{B}$ nonlinearity dominates weakly). This is the spectrum that occurs several eddy turnover times after the initiation of evolution.

transfer well within each subrange continues to be characterized by the transfer of the dominant nonlinearity in isolation. Significant modifications are thus restricted to the crossover region around $\mathbf{k}_0$ where the two nonlinearities are comparable.

(3) The spectrum shift, Eq. (10), affects the transfer in three ways. (a) The spectrum shift contributes to the three-wave-phase decorrelation just as a linear frequency mismatch contributes to the decorrelation. The shift mismatch $\nu_{\mathbf{k}'} + \nu_{\mathbf{k}-\mathbf{k}'} - \upsilon_{\mathbf{k}}$ is finite, because of the dispersion of the shift, and more pronounced for nonlocal triads than local triads. The shift-induced phase decorrelation will therefore limit nonlocal transfer. However, this effect is a factor only in the crossover region. Outside this region, the shift-induced decorrelation is small relative to the phase decorrelation caused by the eddy damping of the dominant nonlinearity. (b) In a strong turbulence regime, the frequency shift in the response function of the driven fluctuation gives rise to a nonresonant contribution [off-diagonal terms in Eq. (10)] to the eddy damping which can, in effect, be comparable to the resonant (diagonal) contribution. In such a case, the transfer, or, equivalently, the energetics, is directly affected by the shift. (c) The frequency shift affects the nonlinear stability (or free-energy extraction) by modifying $\mathrm{Re}\,\omega$ in the eigenmode potential. This effect is most simply displayed in typical drift wave growth rates, which contain the factor $\omega-\omega_*$, with instability for $\omega<\omega_*$. The role of the frequency shift on nonlinear stability, as it pertains to dissipative drift waves, is explored in Ref. 10. As noted previously, this effect is not present in the present computational model but will be examined computationally in a future reference.

It should be apparent from the above that the transfer dynamics of the crossover region is the most difficult to analyze. Figures 4 and 5 depict the evolution of the spectrum in the crossover region under nondriven, nondamped relaxation, with $\mathbf{k}_0$ slightly larger than the median $\mathbf{k}$. Figure 4 is the spectrum a few eddy turnover times after commencing the relaxation from a initial $\mathbf{k}^{-3}$ distribution. Significant nonlocal transfer to high-$\mathbf{k}$ modes is evident in the peaks which have developed at high $|\mathbf{k}|$. This peaking feature is isotropic in $\mathbf{k}$ and contrasts with the peaks that occur at high $\mathbf{k}_y$ (but not $\mathbf{k}_x$) at comparable times with the $\mathbf{E}\times\mathbf{B}$ nonlinearity alone. The nonlocal transfer is an unmistakable signature of the $\mathbf{E}\times\mathbf{B}$ nonlinearity, whereas the tendency toward isotropy is a feature of the polarization drift nonlinearity. Isotropization of the high-k peaks is accomplished by transfer modifications induced by the spectrum distribution (principle 2). The final equilibrium spectrum (Fig. 5) is mostly flat with a narrow peak at low $\mathbf{k}$. The peak is produced by the inverse cascade of the polarization drift nonlinearity. It is more narrow than the peak that occurs with the polarization drift nonlinearity alone (Fig. 1) because of the competing transfer to high $\mathbf{k}$ produced by the $\mathbf{E}\times\mathbf{B}$ nonlinearity. The flat portion is attributable to the $\mathbf{E}\times\mathbf{B}$ nonlinearity, which tends to drive the spectrum to equipartition. In this regard, it is interesting to note that the spectrum predicted by equilibrium statistical mechanics is the equipartitioned spectrum, since enstrophy is not conserved in this case. Statistical mechanics is unable to account for the inverse cascade because the $\mathbf{E}\times\mathbf{B}$ nonlinearity breaks enstrophy invariance even though significant enstrophy-conserving transfer by the polarization drift nonlinearity occurs.

The degree of nonconservation of enstrophy, or, more precisely, the rate of enstrophy generation, is a measure of the extent of energy transfer to high $\mathbf{k}$ by the $\mathbf{E}\times\mathbf{B}$ nonlinearity. In Fig. 6, the enstrophy evolution under nondriven, nondamped relaxation is plotted as a function of time for four spectrum configurations. These are the $\mathbf{E}\times\mathbf{B}$ and polarization subranges, in which $\mathbf{k}_0$ falls at either the extreme low end (polarization subrange) or high end of

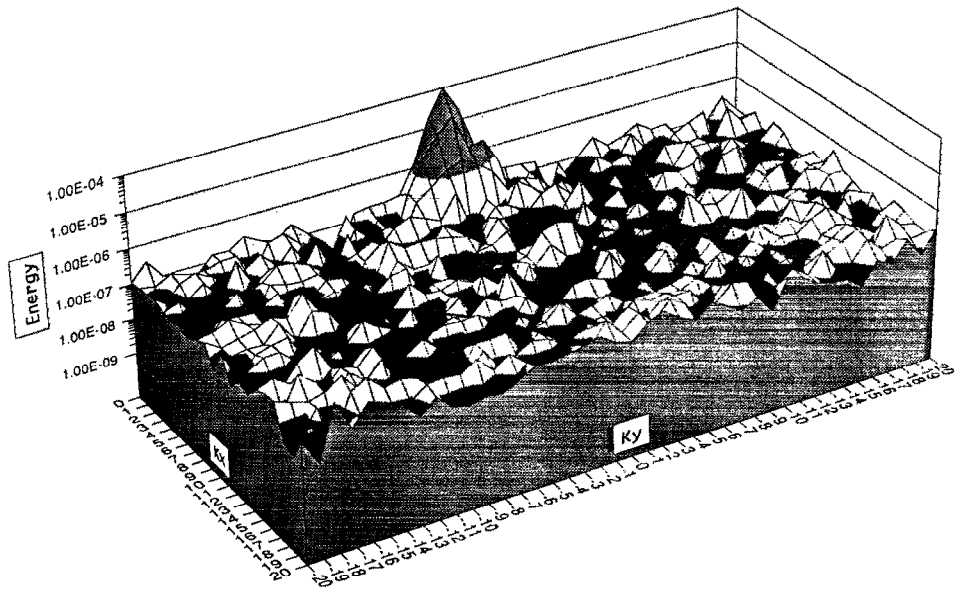

FIG. 5. Final (time asymptotic) spectrum for undriven/undamped turbulence with both the E×B and polarization drift nonlinearities (E×B nonlinearity dominates weakly).

the spectrum (E×B subrange), and two crossover region configurations, one in which k_0 is slightly to the right of center and one in which k_0 falls slightly to the left of center. In the E×B subrange, there is significant enstrophy generation, and the time scale of enstrophy production is a few eddy turnover times. These facts indicate that the transfer dynamics is dominated by the forward cascade of the E×B nonlinearity. In contrast, the small net enstrophy increase and long (many eddy turnover times) generation time scale evident in the polarization subrange indicate that the forward transfer by the E×B nonlinearity is of minor overall importance. In the crossover region, the same general trend is evident, with the net enstrophy production and production rate being roughly proportional to the fraction of k space below k_0. Taken together, these results suggest that, in a spectrum encompassing both subranges, there is significant nonenstrophy-conserving forward transfer from k_{min} to k_0 and somewhat beyond, but that its magnitude relative to the net transfer rapidly diminishes well beyond k_0.

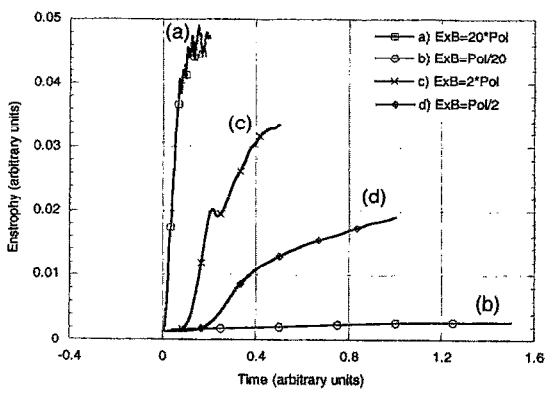

FIG. 6. Time evolution of the enstrophy for four spectrum configurations: (a) spectrum primarily in the E×B subrange, (b) spectrum primarily in the polarization drift subrange, (c) spectrum of crossover region with slightly more of k space below the crossover wave number k_0, and (d) spectrum of crossover region with slightly more of k space above the crossover wave number k_0. The enstrophy production rate is only comparable to the nonlinear interaction (eddy turnover) time in (a) and (c).

It is obviously important to examine the transfer dynamics in a saturated spectrum achieved through the dynamic balance of sources, sinks, and transfer. For dissipative trapped ion convective cells, turbulence is driven at long wavelength (below k_0); at longer wavelengths still, ion–ion collisions provide a sink. The robust forward transfer of the E×B nonlinearity can be expected to carry energy beyond k_0. At some scale, the energy is dissipated (high-k damping). While the existence of a steady state requires a net transfer from sources to sinks, the spectral energy distribution allowing saturation, and the extent of nonlocality and anisotropy in the transfer process must still be determined. In Fig. 7, the stationary spectrum is plotted for a configuration in which k_0 is centrally located between k_{min} and k_{max}. Unstable modes occur in the low-k region with a stable band at the lowest wave numbers, representing ion–ion collisional damping. A broad inertial range extends to the highest wave numbers where a hyperviscous damping provides a high-k sink. Figure 7 reveals a spectrum with sharp peaks at the wave numbers of the driven modes, surrounded by a plateaulike region of roughly elliptical shape. Beyond the plateau, the spectrum falls off sharply to the edge. The edge of the plateau corresponds roughly to the crossover point k_0. Comparison with the stationary spectrum of the E×B nonlinearity alone, which is flat all the way out to the viscously damped modes,[2] indicates that significant nonlocal transfer to high k is the dominant process in the plateau region. Anisotropic trans-

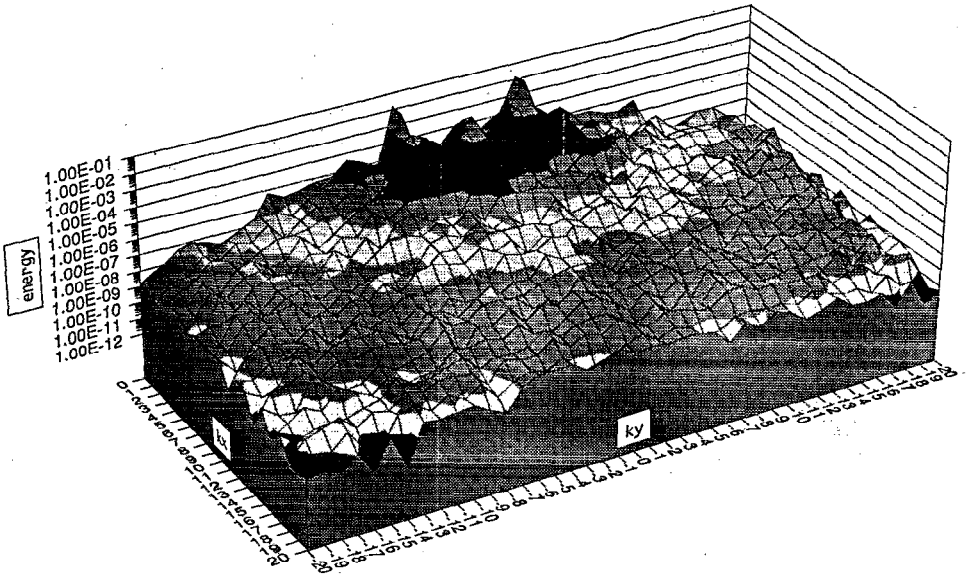

FIG. 7. Spectrum of turbulence driven at long wavelength and damped by a hyperviscosity at short wavelength with an inertial range in the intermediate modes. There is also damping at the smallest wave numbers, representing the effect of ion–ion collisions.

fer is the cause of the elliptical shape of the plateau. There is also transfer to the collisionally damped modes at low **k**, producing a steep drop-off in going below the driven wave numbers. This spectrum indicates that the characteristics of the **E×B** and polarization drift nonlinearities effectively dominate in the appropriate ranges of the spectrum.

The transfer that underlies the spectrum in Fig. 7 is graphically visualized by applying an energy impulse at a specified wave number and observing the subsequent spectrum evolution as it relaxes back to its stationary state. To interpret this diagnostic in cases with both the nonlinearities present, it is helpful to apply it first to the saturated spectra of each nonlinearity in isolation. Figure 8 illustrates the relaxation of the spectrum under the **E×B** nonlinearity starting from the stationary spectrum with a large impulse (red in color) localized to a rectangular annulus in **k** space. Shortly after the impulse, prompt nonlocal transfer carries the energy to all parts of the spectrum. The filamentary structure indicates anisotropic transfer. In the last frame, the stationary spectrum is reestablished at the original level. (To optimize contrast, the color scale in the first frames is different from that of later frames.) In contrast, the same experiment with the polarization drift nonlinearity produces a slower diffusivelike spreading of energy in **k** space, with the inverse cascade restoring the central peak, as shown in Fig. 9. When both nonlinearities are combined, as in Fig. 10, an impulse in the **E×B** subrange produces prompt nonlocal but isotropic transfer

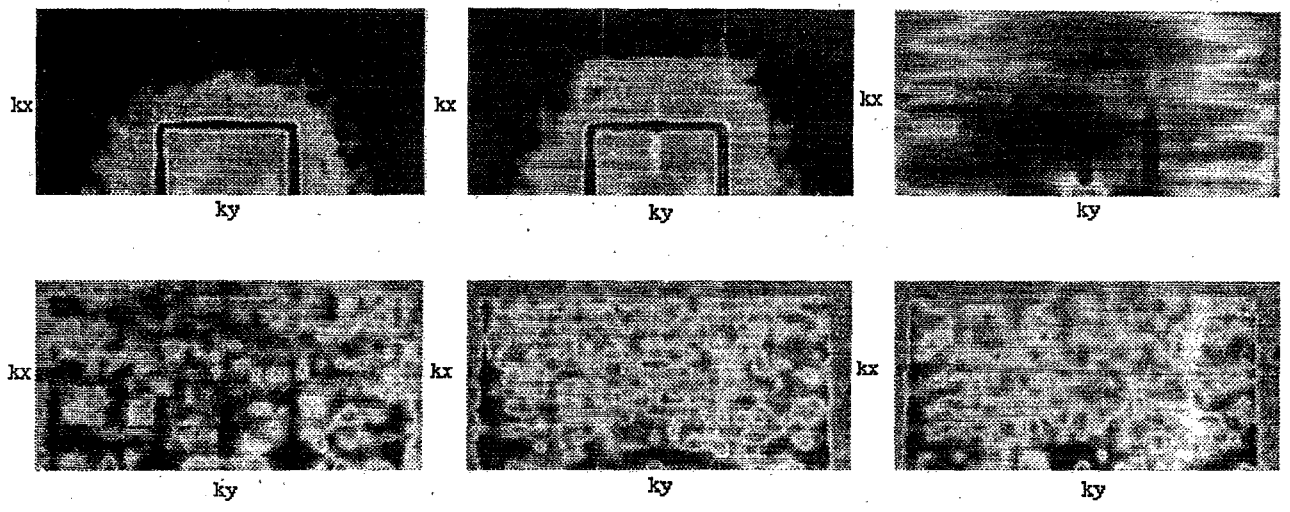

FIG. 8. Evolution of the spectrum with driving and damping (under the **E×B** nonlinearity only) subsequent to an impulse of energy localized to a rectangular annulus in **k** space. Time goes sequentially from left to right and down. The 0,0 mode is at the center bottom of each snapshot and the scale is from red signifying the most energy to purple signifying the least energy.

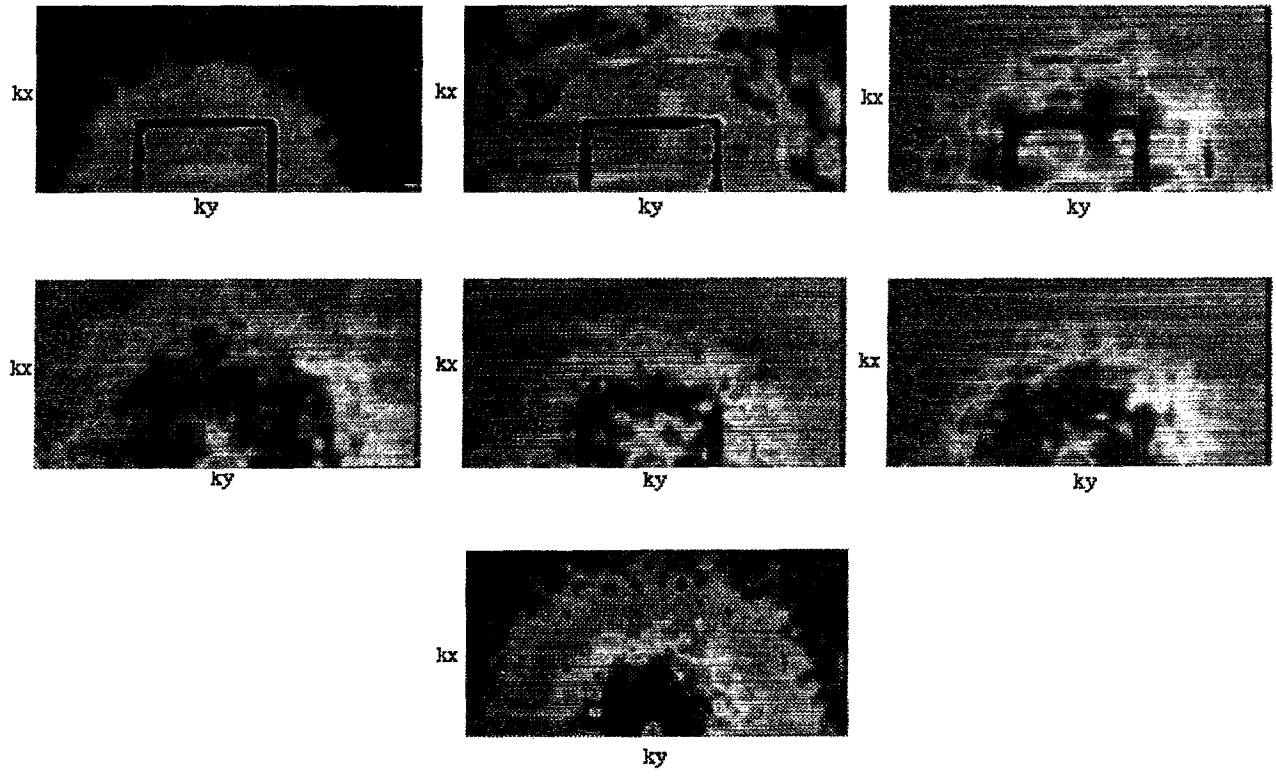

FIG. 9. Evolution of the spectrum with driving and damping (under the polarization drift nonlinearity only) subsequent to an impulse of energy localized to a rectangular annulus in **k** space. Time goes sequentially from left to right and down. The 0,0 mode is at the center bottom of each snapshot and the scale is from red signifying the most energy to purple signifying the least energy.

throughout the spectrum. Subsequent frames show a slower diffusive inverse cascade which restores the central peak. In Fig. 11, the impulse is applied at high **k** in the polarization subrange. The spreading of energy is slower and diffusive throughout the evolution. It is readily apparent that when both nonlinearities are combined, the relaxation of the impulse (at least initially) carries the unmistakable signature of the subrange in which the impulse originates.

IV. FREQUENCY SPECTRUM

The frequency spectrum is generally taken to signify the frequency-dependent part of the power spectrum $S_{\mathbf{k}}(\omega)$, for **k** fixed. In terms of the solution of a spectral representation of the model, i.e., the solution of Eq. (5), the frequency spectrum is just the Fourier transform of the temporal autocorrelation function, obtained from the time history of the mode **k**,

$$S_{\mathbf{k}}(\omega)=\frac{1}{\sqrt{2\pi}}\int d\tau \exp(-i\omega\tau)\langle \tilde{n}_{\mathbf{k}}(t')\tilde{n}_{\mathbf{k}}^{*}(t'+\tau)\rangle, \tag{16}$$

where $\langle\ \rangle$ is the average over a suitably chosen ensemble.

In this section, frequency spectra are examined for a variety of modes and conditions with the objective of establishing qualitatively the existence of a frequency shift induced by the coupling of the $\mathbf{E}\times\mathbf{B}$ and polarization drift nonlinearities. From Eq. (9), it is apparent that the spectrum will contain a shift, given by Eq. (11). However, it should also be noted that the spectrum is a correlation, and the correlation of $\tilde{n}_{\mathbf{k}}(t')$ with $\tilde{n}_{\mathbf{k}}^{*}(t'+\tau)$ for small time differences τ is not captured by simply substituting into Eq. (16) the solution of Eq. (9), an approximate one-time, one-point equation.[13] Specifically, Eq. (9) represents the coherent response, but does not capture the incoherent emission associated with small-scale, short-time correlation. While the *dissipative part* of the incoherent emission ultimately balances the coherent decay in a steady-state inertial range, and thus provides a link between the two components (and a way of determining the linewidth[14]), the reactive component of the incoherent emission is not related to the reactive part of the coherent response, Im $\nu_{\mathbf{k}}$, in any simple way. Thus it is simplistic to expect that the frequency spectrum, and the frequency shift in particular, are totally described by the solution of Eq. (11).[15] Indeed, as will be apparent, the frequency spectra are complicated and not readily interpreted as a localized, single-peaked function. Nevertheless it *is* apparent that a large shift in the mean frequency of the spectrum occurs, that the shift requires the presence of both nonlinearities, and that other features of Eq. (11) are present.

The frequency spectra of both saturated (driven/damped) turbulence and relaxing (no driving or damping) turbulence have been determined. In general, the spectra of saturated turbulence are much broader than the spectra of

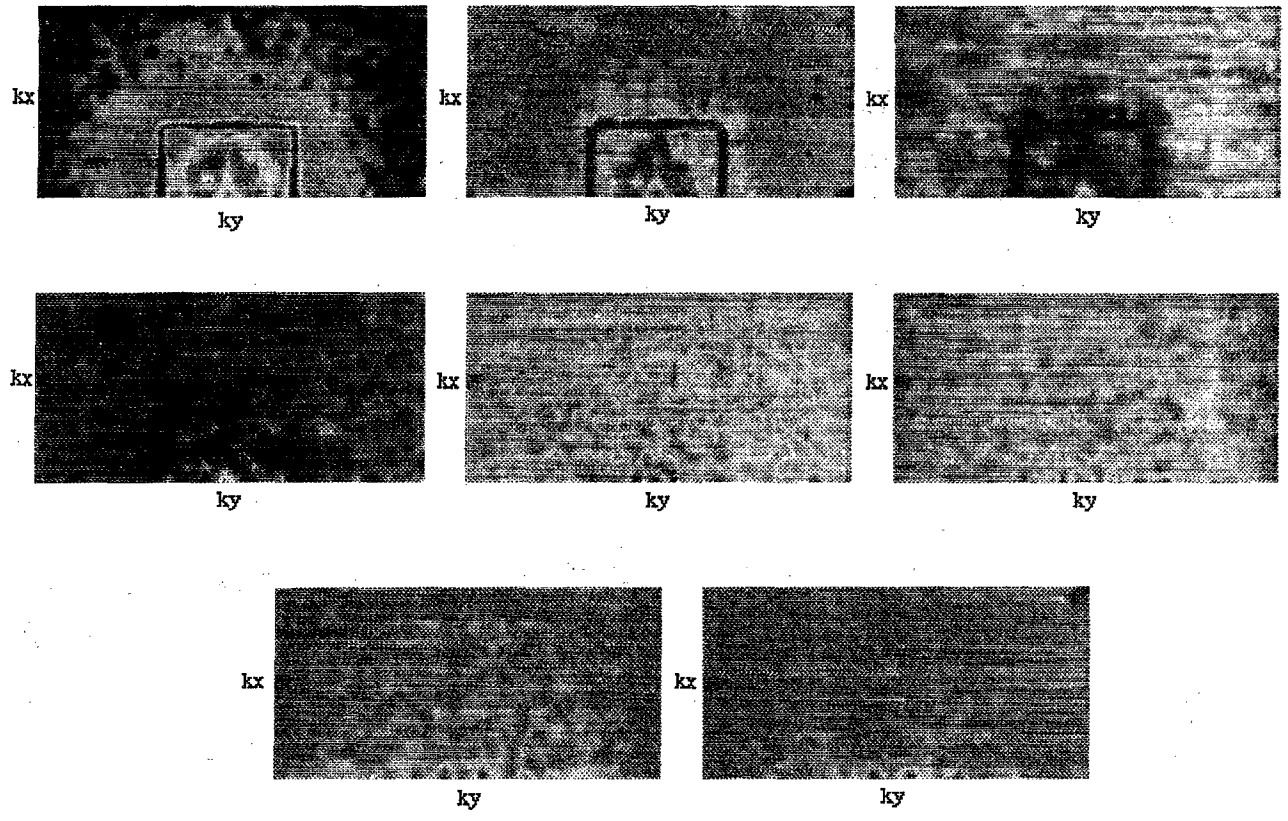

FIG. 10. Evolution of the spectrum with driving and damping and both nonlinearities subsequent to an impulse of energy localized to a rectangular annulus at low k in the E×B subrange. Time goes sequentially from left to right and down. The 0,0 mode is at the center bottom of each snapshot and the scale is from red signifying the most energy to purple signifying the least energy.

relaxing turbulence, and the shifts relative to the linewidths are accordingly less pronounced. The spectra of relaxing turbulence, on the other hand, are not stationary. Computing the spectra from a time history that covers the entire relaxation phase, these spectra have a feature associated with the relaxation. Since the relaxation takes many eddy turnover times, and the time scale of the shift is typically less than an eddy turnover time, the nonstationarity of the spectrum poses no particular difficulty in examining the shifts. At most, the nonstationarity is responsible for intrinsic broadening of the spectrum, but by an amount that is small relative to the magnitude of the shifts. For the above reasons, the spectra shown in the figures are for relaxing turbulence.

Figure 12 shows the frequency spectra of a mode with small wave number for relaxing turbulence with the E×B nonlinearity only, the polarization drift nonlinearity only, and both nonlinearities. In the latter case there is a marked shift of the spectrum peak to higher frequency. In all cases, the peaks are in the electron diamagnetic direction. In Fig. 13, the spectra for a mode with large wave number are displayed. For the cases with E×B and polarization drift nonlinearities only, the spectra are peaked at the small frequency corresponding to the (linear) diamagnetic rotation [third term, Eq. (5)]. With the two nonlinearities combined, the spectrum becomes highly complicated, acquiring a small reproducible feature in the ion direction, and a much larger feature at high frequency in the electron direction. The mean frequency $\bar{\omega}_{\mathbf{k}}=\int d\omega\, \omega S_{\mathbf{k}}(\omega)$ is dramatically raised, as is the width, $\Delta\bar{\omega}_{\mathbf{k}}^2=\int d\omega(\omega^2-\bar{\omega}_{\mathbf{k}}^2)S_{\mathbf{k}}(\omega)$, relative to the cases with a single nonlinearity. For the combined case of Fig. (13), $\bar{\omega}_{\mathbf{k}}\cong 2\Delta\omega_{\mathbf{k}}$. From these figures, it is clear that there is a marked frequency shift associated with the coexistence of the two nonlinearities. The magnitude of the shift, in absolute terms, is larger for the mode with larger wave number. For the shifted spectra of Figs. 12 and 13, $\bar{\omega}_{\mathbf{k}\,\text{large}}/\bar{\omega}_{\mathbf{k}\,\text{small}}\approx 25$, a number of the same magnitude as the ratio of the wave numbers. Both of these features are consistent with the shift described by Eq. (13). The same general features are also found in the spectra of steady-state (driven/damped) turbulence computed numerically for the same model. However, because of the very broad linewidths of the steady-state case, these features are less pronounced.

Given the complexity of the frequency spectrum, especially for high k, a more quantitative comparison with theory is beyond the scope of the present work. Future work will focus on a theoretical understanding of the complex features and inclusion of the feedback of spectrum shifts on the mode stability in the simulations. The existence of a large frequency shift at the longer wavelengths required for the E×B nonlinearity is interesting in light of the apparent observation of long-wavelength fluctuations with large phase velocity ($v_{\text{ph}}>\omega_*/\mathbf{k}$) in the Texas Experimental Tokamak (TEXT).[16]

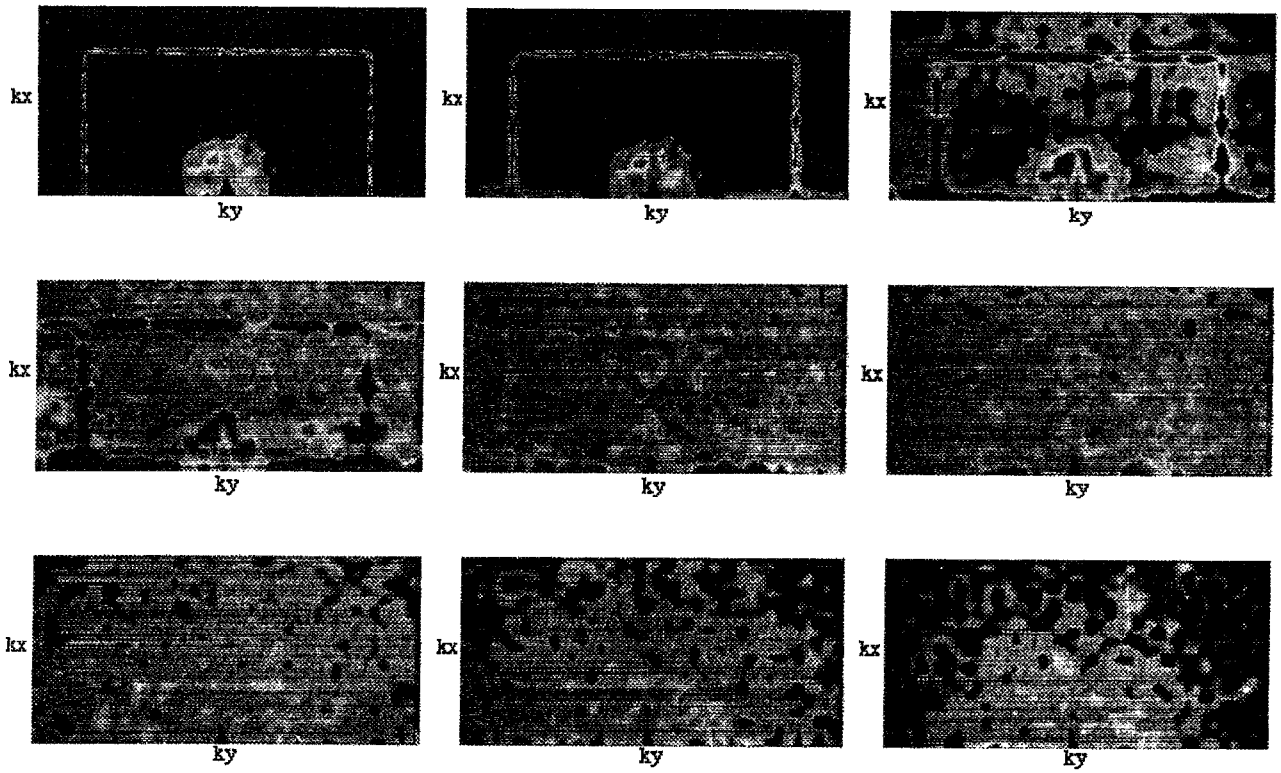

FIG. 11. Evolution of the spectrum with driving and damping and both nonlinearities subsequent to an impulse of energy localized to a rectangular annulus at high k in the polarization drift subrange. Time goes sequentially from left to right and down. The 0,0 mode is at the center bottom of each snapshot and the scale is from red signifying the most energy to purple signifying the least energy.

V. CONCLUSIONS

The spectral transfer dynamics of drift wave turbulence over the broad wave-number range incorporating both the E×B and polarization drift nonlinearities has been explored. This work is based on numerical solution of the single-field dissipative trapped ion convective cell turbulence model[1,2] and describes the spectral transfer resulting from unstable trapped ion modes at long wavelength. Related analytical work is contained in the accompanying paper (Ref. 13). The present computational model is based on an "$i\delta$" approximation with laminar electron dynamics resulting from collisional, nonadiabatic electrons. Consequently, the present computational model neglects the dynamical feedback of finite-amplitude nonlinear-induced frequencies on mode stability.

A variety of diagnostics, including wave-number and

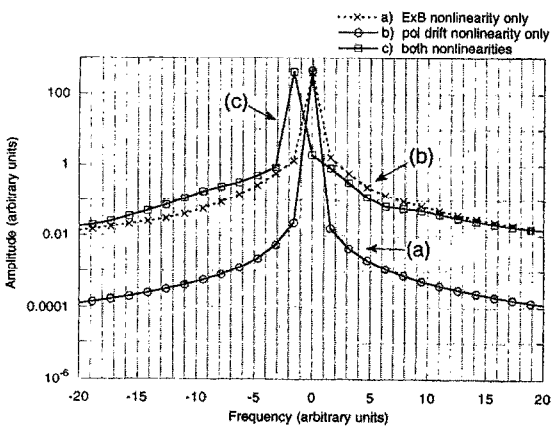

FIG. 12. Frequency spectra of a mode with small wave number during relaxation without driving or damping. The spectra correspond to (a) E×B nonlinearity only, (b) polarization drift nonlinearity only, and (c) both nonlinearities.

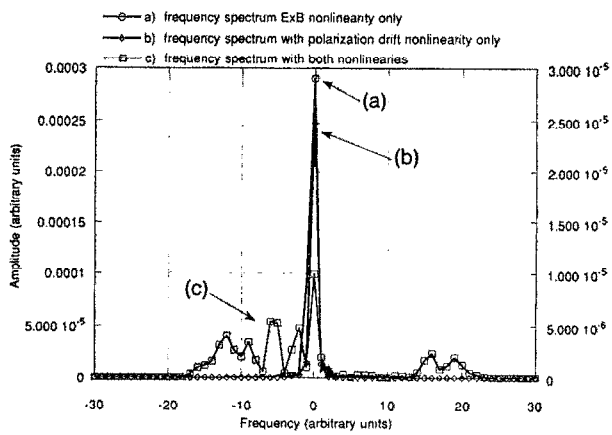

FIG. 13. Frequency spectra of a mode with large wave number during relaxation without driving or damping. The spectra correspond to (a) E×B nonlinearity only, (b) polarization drift nonlinearity only, and (c) both nonlinearities.

frequency spectra, spectrum histories, energy and enstrophy transfer rates, and spectrum impulses, are employed to characterize the transfer. It is found that the $\mathbf{E}\times\mathbf{B}$ and polarization drift nonlinearities transfer energy (and enstrophy) much as they would in isolation. Consequently, there are two subranges corresponding to spectral regions in which one nonlinearity or the other is dominant. In the low-k $\mathbf{E}\times\mathbf{B}$ subrange, the net energy transfer is directed to higher $\mathbf{k}$ with a very large nonlocal component in the $\mathbf{k}_y$ direction. There is significant generation of enstrophy on the time scale of a few eddy turnover times. In the high-k polarization drift subrange, transfer is local in $\mathbf{k}$. There is evidence for a dual cascade, and enstrophy generation is weak, requiring many eddy turnover times for any change in magnitude. The near conservation of enstrophy on dynamical time scales is consistent with the observed inverse cascade of energy. For saturated turbulence that is driven at low $\mathbf{k}$, damped at lower $\mathbf{k}$ and at high $\mathbf{k}$, with an inertial range providing a bridge between the driven wave numbers and the short-wavelength damping, the spectrum is flat in the $\mathbf{E}\times\mathbf{B}$ subrange and falls off in the polarization drift subrange. Nonlocal transfer is responsible for the flatness of the spectrum at low $\mathbf{k}$.

In the crossover region where the two nonlinearities are comparable, there is a rich cross coupling. Energy is transferred nonlocally but the transfer tends to be isotropic. A significant shift in the peak of the frequency spectrum occurs. This shift is directly attributable to the coupling of the two nonlinearities, as it disappears if either nonlinearity is set to zero. The shift increases with increasing wave number. Both of these effects are consistent with the theoretical shift based on the cross coupling of the two nonlinearities in the renormalized response function. In the present work, model limitations have prevented treatment of the back reaction of the shift on the mode dynamics.

The visualization of energy flow by following the spectral relaxation after application of a localized impulse energy at a given wave number is found to provide a reliable and graphic indication of energy flow, indicating accurately its direction, its locality in wave-number space, and whether transfer is isotropic.

Future work on this model will include the frequency shift feedback and its modification of the mode stability structure. In addition, an investigation will be made of structures which are stable solutions of one nonlinearity and their persistence in the presence of both nonlinearities.

ACKNOWLEDGMENTS

The authors acknowledge useful and stimulating discussions with members of the Core Fluctuations Working Group of the Transport Task Force.

This work was supported by U.S. Department of Energy Contracts No. DE-FG02-89ER-53291 and No. DE-FG03-88ER-53275. PHD would like to acknowledge support from an Alfred P. Sloan Foundation Fellowship and a N.S.F. Presidential Young Investigator Award. In producing the color figures, the use of Image and Layout by the National Center for Supercomputing Applications at the University of Illinois at Urbana–Champaign is also acknowledged.

[1]P. H. Diamond and H. Biglari, Phys. Rev. Lett. **65**, 2865 (1990).
[2]D. E. Newman, P. W. Terry, and P. H. Diamond, Phys. Fluids B **4**, 599 (1992).
[3]R. J. Fonck, S. F. Paul, D. R. Roberts, Y. J. Kim, N. Bretz, D. Johnson, R. Nazikian, and G. Taylor, in *18th European Conference of Controlled Fusion and Plasma Physics*, Berlin, Germany, edited by P. Bachmann and D. C. Robinson (European Physical Society, Geneva, 1991), Vol. 15C, Part I, p. I-269.
[4]P. Cripwell and A. E. Costley, in Ref. 3, p. I-17.
[5]P. M. Schoch, J. C. Forster, W. C. Jennings, and R. L. Hickok, Rev. Sci. Instrum. **59**, 1825 (1986).
[6]D. L. Brower, W. A. Peebles, and N. C. Luhmann, Nucl. Fusion **27**, 2055 (1987).
[7]P. W. Terry and W. Horton, Phys. Fluids **25**, 491 (1982).
[8]A. Hasegawa and K. Mima, Phys. Rev. Lett. **39**, 205 (1977).
[9]R. H. Kraichnan, J. Fluid Mech. **47**, Part 3, 525 (1971).
[10]Y.-M. Liang, P. H. Diamond, X. H. Wang, D. E. Newman, and P. W. Terry, Phys. Fluids B **5**, 1128 (1993).
[11]P. W. Terry and P. H. Diamond, in *Statistical Physics and Chaos in Fusion Plasmas*, edited by W. Horton and L. Reichl (Wiley, New York, 1984), p. 335; P. W. Terry and P. H. Diamond, Phys. Fluids **28**, 1419 (1985).
[12]P. W. Terry and D. E. Newman, Bull. Am. Phys. Soc. **37**, 1475 (1992).
[13]T. Boutros-Ghali and T. H. Dupree, Phys. Fluids **24**, 1839 (1981).
[14]The linewidth is not directly given by the coherent damping. In steady state, coherent damping is balanced by driving and incoherent emission and all of these processes affect the spectrum. This is discussed in the articles of Ref. 11.
[15]This is further discussed in N. Mattor and P. W. Terry, Phys. Fluids B **4**, 1126 (1992).
[16]D. W. Ross, R. V. Bravenec, C. P. Ritz, M. L. Sloan, J. R. Thompson, A. J. Wootton, P. M. Schoch, J. W. Heard, T. P. Crowley, R. L. Hickok, V. Simcic, D. L. Brower, W. A. Peebles, and N. C. Luhmann, Jr., Phys. Fluids B **3**, 2251 (1991).